

Article

Statistical Modeling of Photo-Bending Actuation of Hybrid Silicones Mixed with Azobenzene Powder

Takuya Taniguchi ^{1,*}, Loïc Blanc ², Toru Asahi ^{3,4}, Hideko Koshima ⁴ and Pierre Lambert ^{2,*} ¹ Center for Data Science, Waseda University, 27 Waseda-cho, Shinjuku-ku, Tokyo 169-0042, Japan² TIPs Department, CP165/67, Université libre de Bruxelles, 50 Av. Franklin Roosevelt, 1050 Brussels, Belgium; Loic.Blanc@ulb.ac.be³ Department of Life Science and Medical Bioscience, Graduated School of Advanced Science and Engineering, Waseda University, 2-2 Wakamatsu-cho, Shinjuku-ku, Tokyo 169-8480, Japan; tasahi@waseda.jp⁴ Research Organization for Nano & Life Innovation, Waseda University, 513 Wasedaturumaki-cho, Shinjuku-ku, Tokyo 162-0041, Japan; h.koshima@kurenai.waseda.jp

* Correspondence: takuya.taniguchi@aoni.waseda.jp (T.T.); pierre.lambert@ulb.ac.be (P.L.)

Received: 6 September 2019; Accepted: 18 September 2019; Published: 20 September 2019



Abstract: Mechanically responsive materials are promising as next-generation actuators for soft robotics, but have scarce reports on the statistical modeling of the actuation behavior. This research reports on the development and modeling of the photomechanical bending behavior of hybrid silicones mixed with azobenzene powder. The photo-responsive hybrid silicone bends away from the light source upon light irradiation when a thin paper is attached on the hybrid silicone. The time courses of bending behaviors were fitted well with exponential models with a time variable, affording fitting constants at each experimental condition. These fitted parameters were further modeled using the analysis of variance (ANOVA). Cubic models were proposed for both the photo-bending and unbending processes, which were parameterized by the powder ratio and the light intensity. This modeling process allows such photo-responsive materials to be controlled as actuators, and will possibly be effective for engineering mechanically responsive materials.

Keywords: photo-actuation; statistical modeling; bending behavior; hybrid silicone; azobenzene powder

1. Introduction

The word “robot” was born in a play written by Karel Čapek nearly a hundred years ago [1]. Since then, robots have been utilized in many industries owing to their automated and precise manipulations, planting the impression that robots have hard bodies. More recently, in contrast to hard-bodied robots, soft robotics has emerged as a research field, because soft-bodied robots, which are basically made of polymers, are adaptable to their external environment, enabling safe human contact and grip objects [2]. Currently, the working mechanism of soft robots is mostly based on pneumatic pressure due to the advantage of large output force [3,4]. However, pneumatic actuation requires a large pressure pump, and is sometimes difficult to downscale (especially valves). As expectations for soft robots are increasing, the development of new soft actuation systems will lead to diversifying types of soft robots working in different environments.

Mechanically responsive organic materials are expected as next-generation actuators, potentially implemented in soft robots and flexible devices [5,6]. These materials actuate responding to external stimuli, such as light, heat, magnetic field, voltage, and humidity [7]. Among them, photo-actuation is attractive from the viewpoint of non-contact actuation in focused place and faster space transmission of light. Many photomechanical materials have been developed thus far. For example, polymers

and gels chemically bridged with photo-reactive molecules, such as typical photochromic compound azobenzene, can deform upon light irradiation due to *trans-cis* photoisomerization [8–11]. In addition, the past decade has witnessed mechanical responses of photo-responsive organic crystals, overturning the stereotypic concept that crystals are solid and fragile materials [12–16]. The photo-actuation variety of materials has motivated us to combine the flexibility of polymeric materials with the bendable feature of organic crystals for the development of photo-responsive hybrid materials. Up to the current status, hybrid materials have been fabricated based on the crystallization of photo-reactive powders in polymers [17–20], the inclusion of photomechanical bulk crystals into polymers [21], and the mixing of composites for photothermal actuation [22–28]. Such hybrid materials are promising as photo-actuators due to the simplicity of the fabrication process and the ease of size and shape control. With these advantages, it is crucial to describe actuation behavior in a mathematical model for controlling the output. There have been reports on the theoretical models of photo-actuation [29–32]; however, there are scarce reports on the statistical modeling based on experimental results, which is effective to optimize their photo-actuation behaviors.

This work reports on the strategy from the development of photo-responsive hybrid silicones containing azobenzene compounds to the statistical modeling of photo-bending and unbending behaviors. The hybrid silicones are fabricated by mixing photo-reactive compound azobenzene at different weight contents into silicones. The fabricated hybrid silicones exhibit the photomechanical responses; elongation if free to expand, and bending when constrained by a paper strip. The bending behaviors are observed at various conditions, and then modeled by a statistical analysis of variance (ANOVA). This strategy of modeling photo-actuation behavior should be applied to the optimization of the other properties of photo-responsive hybrid materials.

2. Materials and Methods

A rectangular plate-like mold made of polylactic acid (PLA) was prepared by using a three-dimensional (3D) printer (Makerbot Replicator). The size of the mold was 40 mm long, 30 mm wide, and 1 mm thick. Silicone (Ecoflex 00-50, Smooth-on) was poured into the mold as the first layer, and then cured at room temperature by overnight (Figure 1a). Next, 4-aminoazobenzene powder (as purchased from Sigma-Aldrich) was mixed into raw uncured silicone with different weight ratios (0, 1, 5, and 10 wt%) to the weight of the second layer. Note that 0 wt% means pure silicone. The uncured silicone containing azobenzene powder was coated as the second layer onto the cured silicone in the mold (Figure 1b). After curing, the hybrid silicone containing azobenzene compound was detached from the mold (Figure 1c). Here, the whole material has an orange coloration, which corresponds to the color of the azobenzene compound, due to diffusion from the second layer. Then, the hybrid silicone was cut along the length to prepare for samples with narrower width suitable for observations (Figure 1d, and see supplementary information for more detailed procedure). We define the second layer surface as the front side and the opposite side as the back side of the hybrid silicone.

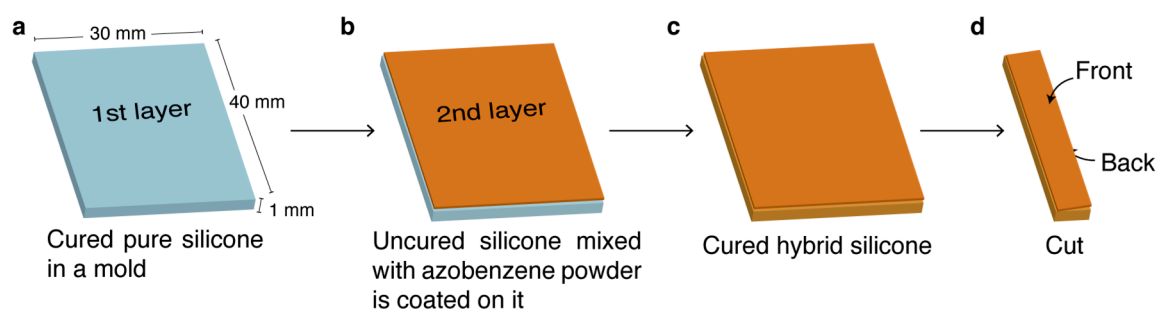


Figure 1. Preparation of a hybrid silicone mixed with azobenzene powder. (a) Curing the first layer. (b) Coating uncured silicone containing azobenzene powder as the second layer. (c) Obtained hybrid silicone after curing the second layer. (d) Cutting for bending observations.

For observations, a strip-shaped hybrid silicone was fixed to hang down keeping straight shape by its own weight. Ultraviolet (UV) light at 365 nm was irradiated to the front side of the hybrid silicone with a certain distance by using a UV light emitting diode, UV-LED (EQ CL25, LOCTITE) without a focusing lens. The net light intensity to a sample was 150, 300, 450, and 600 mW/cm² by changing the controller power 25, 50, 75, and 100%. The bending and unbending behaviors of hybrid silicones (0, 1, 5, and 10 wt%) were observed by turning on UV light for 3 min and turning it off for 4 min. This observation was repeated three times in each condition. Such repetitive observations were performed at each light intensity (150, 300, 450, or 600 mW/cm²). The movies were recorded by a personal smartphone (iPhone X, Apple). The bending deflection was calculated from the recorded movies by using software ImageJ. The experimental results of deflections were fitted with an exponential function for bending and unbending each by using solver function in excel ver. 16.16.2 (Microsoft), and then modeled by using a statistical software DesignExpert ver. 11.1.2.0 (Stat-Ease). Model constructions are tested by linear, two factor interaction (2FI), quadratic, cubic, and quartic functions. These functions are represented as combinations of two variables x_1 and x_2 corresponding to the percentage of the powder content and the UV intensity (Table 1).

Table 1. Combination of variables in model functions.

	x_1	x_2	x_1x_2	x_1^2	x_2^2	$x_1^2x_2$	$x_1x_2^2$	x_1^3	x_2^3	$x_1^2x_2^2$	$x_1^3x_2$	$x_1x_2^3$	x_1^4	x_2^4
Linear	Y	Y	-	-	-	-	-	-	-	-	-	-	-	-
2FI	Y	Y	Y	-	-	-	-	-	-	-	-	-	-	-
Quadratic	Y	Y	Y	Y	Y	Y	Y	-	-	-	-	-	-	-
Cubic	Y	Y	Y	Y	Y	Y	Y	Y	Y	-	-	-	-	-
Quartic	Y	Y	Y	Y	Y	Y	Y	Y	Y	Y	Y	Y	Y	Y

(If a variable is considered, Y = yes, - = no).

3. Results & Discussions

3.1. Photo-Actuation Behavior

The sizes of fabricated hybrid silicones used for observations are summarized in Table 2. When a strip-shaped hybrid silicone of 10 wt% free to expand was irradiated by UV light from the front side, the hybrid silicone just elongated along the length and did not exhibit noticeable bending (Figure 2a). In contrast, when the hybrid silicone of 10 wt% attached with a thin paper at the back side was irradiated by UV light, the sample bent away from the light source, reaching almost a steady state for 3 min irradiation (Figure 2b). Such bending was also observed in a silicone homogeneously mixed with azobenzene powder when constrained by a paper (Supplementary Figure S1). The bending depends on the light direction, the position of the photo-initiators in the structure and the paper strip. Therefore, modifying these parameters would be used to adjust the bending direction.

These photo-responsive behaviors of both elongation and bending originate from the photothermal effect. When a hybrid silicone is irradiated by UV light, the surface temperature of the hybrid silicone rises due to heat generation from azobenzene compounds (Supplementary Figure S2). Without any paper, the temperature on irradiated area rises due to the photothermal effect, and the heat is transmitted into the silicone up to the non-irradiated opposite side, resulting in the elongation of the length due to thermal expansion. By attaching a paper, the irradiated area on the front side also elongates due to thermal expansion, but the elongation on the back side is restricted due to elongation rigidity of the attached paper. This elongation difference between front and back sides results in bending away from the light source, and will be measured here by the tip deflection δ (see Figure 2). The photo-actuation behaviors, the elongation, if free to expand, and the bending when constrained by a paper strip, were observed in all hybrid silicones due to the photothermal effect, indicating that pure silicone (0 wt%) has photothermal effect but azobenzene compounds enhance the photothermal effect owing to higher light absorption (Supplementary Figure S2).

Furthermore, the unbending after the removal of UV light was observed to clarify the contribution of photochemical isomerization on the actuation of hybrid silicones. If photochemical isomerization contributes to actuation, the unbending under visible light irradiation should be faster than that without visible light, because visible light accelerates *cis*-to-*trans* back-isomerization photochemically, as reported for the photomechanical crystal of the same compound, 4-animoazobenzene [33]. As the observation result, the unbending under visible light was slower than that without visible light (Supplementary Figure S3). This result indicates that the photochemical isomerization is not dominant effect to actuation; rather, the photothermal effect mainly contributes. The slower unbending under visible light is due to the photothermal effect of azobenzene, which absorbs visible light and generates heat to cause unbending slower. Thus, photo-actuation of these hybrid silicones is based on the photothermal effect.

Table 2. Sizes of silicone strips used for observations.

	0 wt%	1 wt%	5 wt%	10 wt%
Length from irradiated center to the tip/mm	20.0	18.9	18.0	16.5
Width/mm	4.9	4.5	4.9	5.5
Thickness/mm	1.4	1.5	1.7	1.5

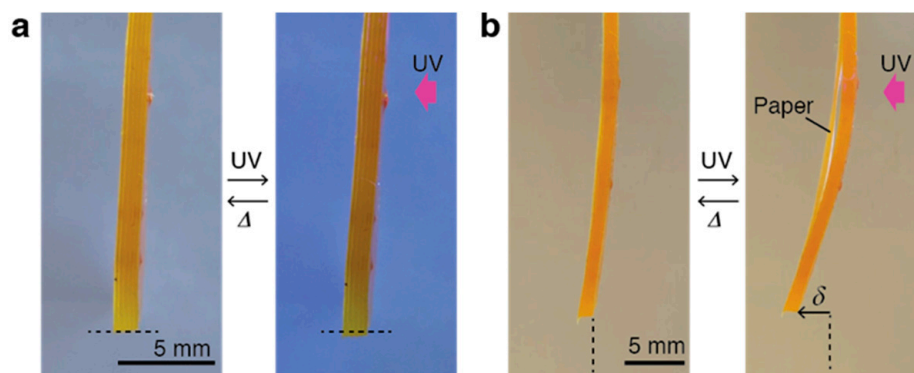


Figure 2. Shape change of a hybrid silicone with azobenzene powder (10 wt%) before and after ultraviolet (UV) light irradiation. (a) Elongation of the hybrid silicone when free to expand. (b) Bending of the hybrid silicone when constrained by a paper. Dotted lines in panels show the initial position before UV irradiation. In both cases, UV light (365 nm) was irradiated 3 min at 600 mW/cm².

3.2. Bending Evaluation

The bending behavior is quantified from the tip deflection δ , which can be extracted from the recorded movies (Figure 2b). The deflection δ can be described as the following equation:

$$\delta = \frac{Fl^3}{3EI}$$

here, F is the bending force, l is the length of an object, E is Young's modulus, and I is the moment of inertia. The moment of inertia I of this beam is expressed as:

$$I = \frac{bh^3}{12}$$

where b is the width, and h is the thickness of the sample. By using these equations, the bending deflection δ can be replaced as a non-dimensional value δ' in the following:

$$\delta' = \frac{\delta h^2}{l^3} = \frac{4F}{Ebh}$$

In this paper, bending behavior was evaluated by this non-dimensional deflection δ' for regularization to compare the different samples with no influence of their dimensions. For l , b , and h , the values in Table 2 were applied at calculations.

The bending and unbending behaviors of hybrid silicones of 0, 1, 5, and 10 wt% constrained by a paper strip on back side were observed while turning on UV light for 3 min and then turning it off for 4 min. The real deflections δ of each observation were summarized in Supplementary Tables S1 and S2, and then were converted into the deflections δ' . Figure 3 shows the time course of the deflection δ' for bending under light irradiation and consecutive unbending after the removal of UV light.

Regarding the photo-bending process, the deflection δ' at each condition increased continuously depending on irradiation time to reach a steady state for 3 min irradiation (Figure 3). Additionally, the maximum deflection increased depending on the increase of light intensity (150, 300, 450, and 600 mW/cm²). The deflection δ' in the photo-bending process at each condition was successfully fitted by least square to an exponential model:

$$\delta'(t) = A \left\{ 1 - \exp\left(-\frac{t}{\tau_b}\right) \right\}$$

where A is the maximum bending deflection at steady state, t is time, and τ_b is the time constant of bending. Constants A and τ_b are obtained from fitting the model, as summarized in Table 3. At a glance, the value A of a hybrid silicone tended to increase for increasing light intensity and powder ratio. For instance, the hybrid silicone of 10 wt% afforded $A = 4.88$ at the intensity 150 mW/cm², and increased up to $A = 13.2$ at the intensity 600 mW/cm². This tendency is applied to other hybrid silicones of 0, 1 and 5 wt%. As to the value of τ_b , it decreased for increasing light intensity, but there was no clear relation with the amount of powder contents.

Regarding the unbending process, the deflection δ' at each condition decreased continuously depending on time after the removal of UV light (Figure 3). The deflections δ' in the unbending process at each condition was successfully fitted by least square to a decreasing exponential model:

$$\delta'(t) = A \exp\left(-\frac{t}{\tau_u}\right)$$

where A is the maximum deflection (i.e., initial deflection for unbending), τ_u is a time constant for unbending, and t is the time after stopping light irradiation. The values of A and τ_u for unbending are summarized in Table 4. Since the maximum deflection is determined in photo-irradiated process, the values A for unbending are almost same with those for photo-bending in Table 3, although there are slight differences due to fitting. Thus, the unique parameter in the unbending process is the time constant τ_u only. The value τ_u tended to become larger depending on the irradiated light intensity. For example, the hybrid silicone of 10 wt% afforded $\tau_u = 69.0$ s after irradiated at 150 mW/cm² and increased up to $\tau_u = 74.4$ s after irradiated at 600 mW/cm². This tendency was almost observed in the other hybrid silicones (with different powder content), although some conditions of the hybrid silicones of 0 and 1 wt% did not match with the trend. When comparing the samples at the same light intensity, the trend is that higher powder contents lead to higher τ_u values, although the maximum appeared at 5 wt%.

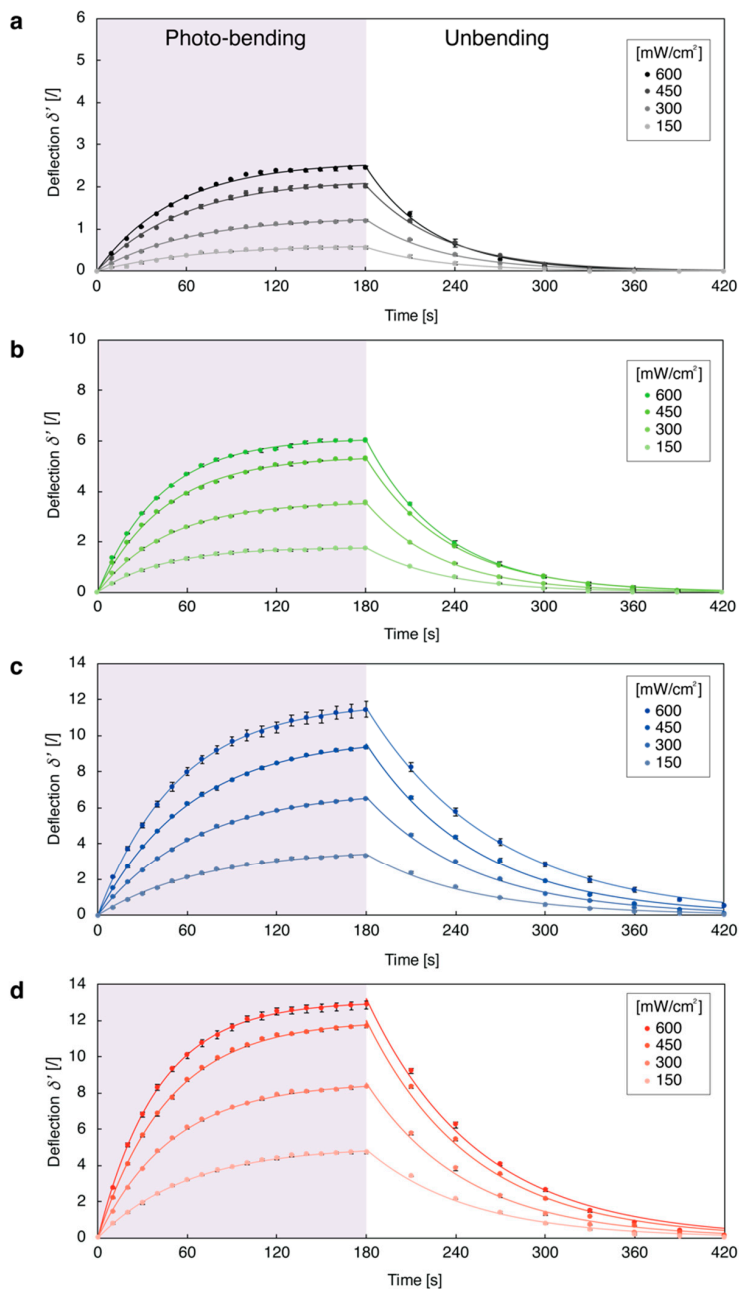


Figure 3. Time dependence of deflection δ' of hybrid silicones under UV light illumination at different light intensities and after stopping the irradiation. Panels show the results of hybrid silicones of (a) 0, (b) 1, (c) 5, and (d) 10 wt%. Plots drawn by small circle indicate the average value of deflection repeatedly observed three times, with standard deviations. Solid lines are the results of fitting to exponential models for photo-bending and unbending processes.

Table 3. Summary of A and τ_b obtained by fitting to the exponential model for photo-bending.

Light (mW/cm ²)	The Value of A				The Value of τ_b			
	0 wt%	1 wt%	5 wt%	10 wt%	0 wt%	1 wt%	5 wt%	10 wt%
150	0.57	1.78	3.41	4.88	66.7	43.6	70.7	60.1
300	1.23	3.57	6.61	8.56	61.6	46.9	65.8	49.8
450	2.04	5.32	9.54	12.0	58.0	45.6	62.1	47.0
600	2.48	6.07	11.5	13.2	52.9	41.8	53.6	40.2

Table 4. Summary of A and τ_u obtained by fitting to the exponential model for unbending.

Light (mW/cm ²)	The Value of A				The Value of τ_u			
	0 wt%	1 wt%	5 wt%	10 wt%	0 wt%	1 wt%	5 wt%	10 wt%
150	0.62	1.78	3.69	5.05	48.7	52.5	70.9	69.0
300	1.28	3.59	6.97	8.60	49.9	50.9	72.4	67.6
450	2.18	6.97	9.91	12.0	51.4	55.5	74.7	71.2
600	2.60	8.60	11.8	13.1	44.7	52.8	85.7	74.4

3.3. Model Construction

3.3.1. Model Construction for Photo-Bending

In order to model the influence on A of the UV power and the percentage of powder, an ANOVA study has been performed according to Fisher's statistical test. As a result of a comparison of some models (linear, 2FI, quadratic, cubic, and quartic), a cubic model is representative as the p -value of this model is 2.18×10^{-6} (significant) and the related lack of fit has a p -value of 0.228 (not significant, which means that the cubic model is adequate enough) as shown in Table 5. For instance, a linear model presents a p -value of 7.49×10^{-19} (also significant), but a lack of fit of 4.86×10^{-15} (significant, which means that this model is not suited to fit the data). A quartic model scores comparable adjusted R^2 and predicted R^2 , but has a p -value of 0.0871 (not significant), showing this quartic model is aliased.

The ANOVA result for A value calculated for the cubic model is summarized in Table 6, indicating the significance of variables. The complete cubic model for the A parameter is given by the following equation:

$$A = 1.73 + 1.54P_{\%} - 1.87 \times 10^{-2}P_{UV} + 4.71 \times 10^{-3}P_{\%}P_{UV} - 0.362P_{\%}^2 + 7.70 \times 10^{-5}P_{UV}^2 - 1.96 \times 10^{-4}P_{\%}^2P_{UV} - 1.99 \times 10^{-6}P_{\%}P_{UV}^2 + 2.19 \times 10^{-2}P_{\%}^3 - 7.19 \times 10^{-8}P_{UV}^3$$

where $P_{\%}$ is the weight percentage of powder (in %) and P_{UV} the intensity of UV light (in mW/cm²). For any parameter to be significant, its F -value should be higher than 0.05 and its p -value should be lower than 0.05. Among variables in the full cubic model, the terms of $P_{\%}$ and P_{UV}^2 are not significant due to p -value larger than 10%, while all the other parameters of the cubic model have a p -value lower than 4.0% (Table 6). This is how the cubic model can slightly be simplified by removing the variables that are not significant. The new proposed model is, therefore:

$$A = 0.315 + 4.79 \times 10^{-3}P_{UV} + 6.37 \times 10^{-3}P_{\%}P_{UV} - 3.29 \times 10^{-2}P_{\%}^2 - 2.89 \times 10^{-4}P_{\%}^2P_{UV} - 2.87 \times 10^{-6}P_{\%}P_{UV}^2 + 2.71 \times 10^{-3}P_{\%}^3 - 7.13 \times 10^{-10}P_{UV}^3$$

All the coefficients of the reduced cubic model have p -values lower than 5.0% and the model itself has a p -value of 8.72×10^{-35} . The two-dimensional (2D) contour plot and 3D response surface of the reduced cubic model is represented in Figure 4. The response surface shows that the value A increases depending on the increase of both the UV intensity and the powder contents.

Table 5. Summary of comparison between models for A obtained from the photo-bending.

Source	Sequential p -Value	Lack of Fit p -Value	Adjusted R^2	Predicted R^2
Linear	7.49×10^{-19}	4.86×10^{-15}	0.837	0.820
2FI	1.42×10^{-4}	4.62×10^{-13}	0.880	0.864
Quadratic	1.09×10^{-12}	4.66×10^{-5}	0.966	0.960
Cubic	2.18×10^{-6}	0.228	0.983	0.977
Quartic	0.0871	0.619	0.985	0.977

Table 6. ANOVA results for A value in the complete cubic model for photo-bending.

Source	Sum of Squares	df	Mean Square	F-Value	p-Value
Model	739.9	9	82.2	311.4	9.14×10^{-33}
$P_{\%}$	0.69	1	0.69	2.6	0.113
P_{UV}	60.6	1	60.6	229.4	1.09×10^{-17}
$P_{\%}P_{UV}$	22.7	1	22.7	86.1	2.62×10^{-11}
$P_{\%}^2$	35.6	1	35.6	134.8	4.60×10^{-14}
P_{UV}^2	0.026	1	0.026	0.099	0.755
$P_{\%}^2P_{UV}$	5.4	1	5.4	20.4	5.98×10^{-5}
$P_{\%}P_{UV}^2$	1.5	1	1.5	5.6	0.0229
$P_{\%}^3$	4.5	1	4.5	17.0	1.93×10^{-4}
P_{UV}^3	1.3	1	1.3	4.8	0.0345
Residual	10.0	38	0.26	-	-
Lack of Fit	2.1	6	0.36	1.45	0.228
Pure Error	7.9	32	0.25	-	-
Corrected Total	749.9	47	-	-	-

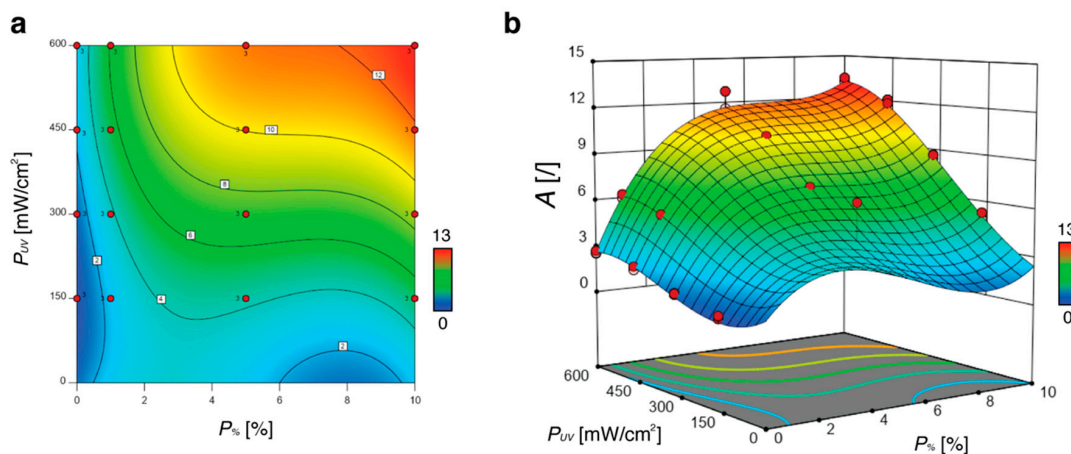


Figure 4. The value A in the photo-bending process, drawn by the reduced cubic model. (a) Contour plot in two dimensions (2D) and (b) surface plot in three dimensions (3D). The dots represent the experimental points (i.e., the fit of the exponential model) and properly fit with the cubic model proposed in this work.

In order to model the influence of the UV intensity and the weight percentage of powder on τ_b , a similar statistical ANOVA study, applied to the τ_b parameter, was performed. A cubic model has also been validated by the statistics as the p -value for this model is 1.76×10^{-11} (significant) and the lack of fit has a p -value of 0.107, meaning not significant (Table 7). For instance, the p -value of the linear model is 1.40×10^{-3} (significant), but the lack of fit is 3.84×10^{-10} (significant) and cannot be used. A quartic model also scores comparable adjusted R^2 and predicted R^2 , but is aliased.

The complete cubic model for the τ_b parameter is given by the following equation:

$$\tau_b = 71.2 - 19.7P_{\%} - 8.29 \times 10^{-2}P_{UV} - 8.15 \times 10^{-3}P_{\%}P_{UV} + 6.83P_{\%}^2 + 2.45 \times 10^{-4}P_{UV}^2 + 4.20 \times 10^{-5}P_{\%}^2P_{UV} + 6.99 \times 10^{-6}P_{\%}P_{UV}^2 - 0.479P_{\%}^3 - 2.56 \times 10^{-7}P_{UV}^3$$

with P_{UV} the power of UV light and $P_{\%}$ the percentage of powder. This model can be simplified by removing the coefficients that are not significant. The terms of P_{UV}^2 , $P_{\%}^2P_{UV}$, $P_{\%}P_{UV}^2$, and P_{UV}^3 are not significant (p -value larger than 30%), while all the other parameters of the cubic model have a p -value lower than 4.5% (Table 8). The new proposed model is, therefore:

$$\tau_b = 67.2 - 20.6P_{\%} - 1.94 \times 10^{-2}P_{UV} - 2.49 \times 10^{-3}P_{\%}P_{UV} + 6.84P_{\%}^2 - 0.479P_{\%}^3$$

All the coefficients of the reduced cubic model have p -values lower than 4.5% and the model it-self has a p -value of 3.33×10^{-16} . The response surface of the new model is presented in Figure 5. The 3D surface shows that the value τ_b at a certain powder content decreases depending on the increase of the light intensity, but the value τ_b is susceptible to the percentage of powder in a not monotonous manner.

As such, both A and τ_b are expressed by the mathematical models, affording the description of the photo-bending behavior of hybrid silicones.

Table 7. Summary of the comparison between models for the τ_b parameter for photo-bending.

Source	Sequential p -Value	Lack of Fit p -Value	Adjusted R^2	Predicted R^2
Linear	0.00140	3.84×10^{-10}	0.220	0.156
2FI	0.202	3.75×10^{-10}	0.232	0.157
Quadratic	0.0253	1.51×10^{-9}	0.324	0.225
Cubic	1.76×10^{-11}	0.107	0.824	0.761
Quartic	0.0186	0.837	0.856	0.785

Table 8. ANOVA results for the τ_b parameter in the complete cubic model for photo-bending.

Source	Sum of Squares	df	Mean Square	F-Value	p -Value
Model	4075.7	9	452.9	25.5	1.77×10^{-13}
$P_{\%}$	1988.5	1	1988.5	112.1	6.84×10^{-13}
P_{UV}	79.1	1	79.1	4.5	0.0413
$P_{\%} P_{UV}$	116.7	1	116.7	6.6	0.0144
$P_{\%}^2$	508.5	1	508.5	28.7	4.38×10^{-6}
P_{UV}^2	9.8	1	9.76	0.55	0.463
$P_{\%}^2 P_{UV}$	0.24	1	0.24	0.01	0.907
$P_{\%} P_{UV}^2$	18.4	1	18.4	1.0	0.315
$P_{\%}^3$	2158.7	1	2158.7	121.7	2.09×10^{-13}
P_{UV}^3	16.1	1	16.1	0.9	0.346
Residual	674.2	38	17.7	-	-
Lack of Fit	178.7	6	29.8	1.92	0.107
Pure Error	495.5	32	15.5	-	-
Corrected Total	4749.9	47	-	-	-

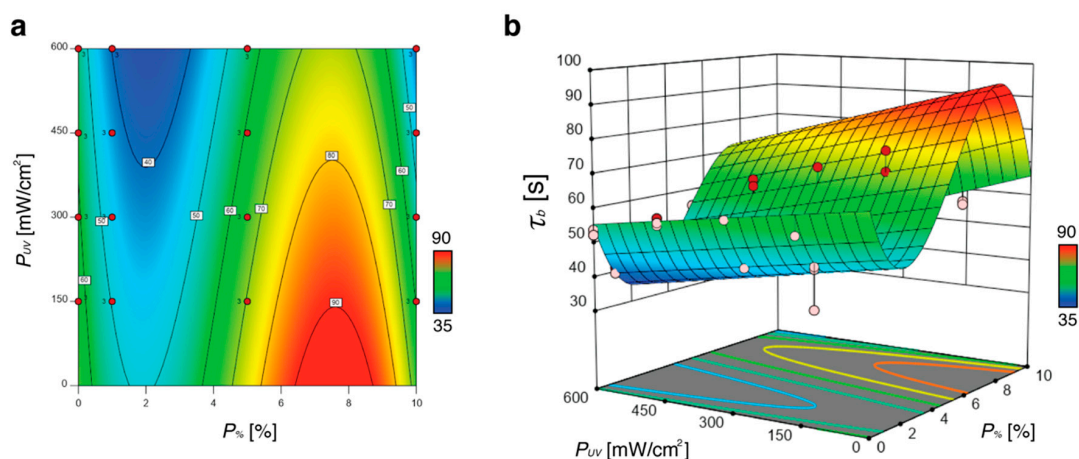


Figure 5. The value τ_b in the photo-bending process, drawn by the reduced cubic model. (a) Contour plot in 2D and (b) surface plot in 3D. The dots represent the experimental data (i.e., the fit of the exponential model). The cubic model gives satisfying fit with these experimental data.

3.3.2. Model Construction for Unbending

Unbending behavior is modeled in the same way. The values of A and τ_u obtained by fitting are summarized in Table 4. The unique parameter in the unbending process is τ_u only, because the value A is determined in the photo-bending process. In order to model the influence of the UV intensity and the weight percentage of powder on τ_u , a statistical ANOVA study, compared to the τ_u parameter, has been performed. Among tested models, a cubic model has also been validated by the statistics as the p -value for this model is 3.64×10^{-4} (significant) and the lack of fit has a p -value of 0.263, meaning not significant (Table 9).

The complete cubic model for the τ_u parameter is given by the following equation:

$$\begin{aligned} \tau_u = & 55.6 + 3.30 \times 10^{-2}P_{\%} - 7.02 \times 10^{-2}P_{UV} + 3.15 \times 10^{-3}P_{\%}P_{UV} + 1.33P_{\%}^2 \\ & + 2.38 \times 10^{-4}P_{UV}^2 - 1.09 \times 10^{-3}P_{\%}^2P_{UV} + 1.30 \times 10^{-5}P_{\%}P_{UV}^2 - 0.104P_{\%}^3 \\ & - 2.45 \times 10^{-7}P_{UV}^3 \end{aligned}$$

with P_{UV} the power of UV light and $P_{\%}$ the percentage of powder. This model can be simplified by removing the coefficient that are not significant (Table 10). The terms of $P_{\%}P_{UV}$, P_{UV}^2 and P_{UV}^3 are not significant (p -value larger than 25%), while all the other parameters of the cubic model have a p -value lower than 3.5%. The new proposed model is, therefore:

$$\begin{aligned} \tau_u = & 49.8 - 1.28P_{\%} - 2.82 \times 10^{-3}P_{UV} + 1.21P_{\%}^2 - 7.72 \times 10^{-4}P_{\%}^2P_{UV} + 1.30 \times 10^{-5}P_{\%}P_{UV}^2 \\ & - 0.104P_{\%}^3 \end{aligned}$$

All the coefficients of the reduced cubic model have p -values lower than 3.5% and the model itself has a p -value of 1.18×10^{-21} . The response surface of the new model is presented in Figure 6, showing that the value τ_u increases depending on the percentage of powder. Thus, the unbending behavior of hybrid silicones has also been expressed as an experiments-based mathematical model.

Table 9. Summary of the comparison between models for the τ_u parameter for unbending.

Source	Sequential p -Value	Lack of Fit p -Value	Adjusted R^2	Predicted R^2
Linear	2.26×10^{-9}	1.85×10^{-10}	0.569	0.531
2FI	0.277	1.54×10^{-10}	0.571	0.528
Quadratic	5.88×10^{-12}	0.00260	0.869	0.844
Cubic	3.64×10^{-4}	0.263	0.915	0.888
Quartic	0.144	0.493	0.921	0.884

Table 10. ANOVA results for the τ_u parameter in the complete cubic model for unbending.

Source	Sum of Squares	df	Mean Square	F-Value	p -Value
Model	6718.9	9	746.5	57.05	2.53×10^{-19}
$P_{\%}$	311.3	1	311.3	23.79	1.95×10^{-5}
P_{UV}	159.7	1	159.7	12.21	0.00123
$P_{\%}P_{UV}$	0.010	1	0.010	0.0	0.978
$P_{\%}^2$	1313.2	1	1313.2	100.34	3.26×10^{-12}
P_{UV}^2	27.3	1	27.3	2.08	0.157
$P_{\%}^2P_{UV}$	168.3	1	168.3	12.86	9.44×10^{-4}
$P_{\%}P_{UV}^2$	64.0	1	64.0	4.89	0.0331
$P_{\%}^3$	101.8	1	101.8	7.78	0.00823
P_{UV}^3	14.8	1	14.8	1.13	0.294
Residual	497.3	38	13.1	-	-
Lack of Fit	100.7	6	16.8	1.35	0.263
Pure Error	396.6	32	12.4	-	-
Corrected Total	7216.2	47	-	-	-

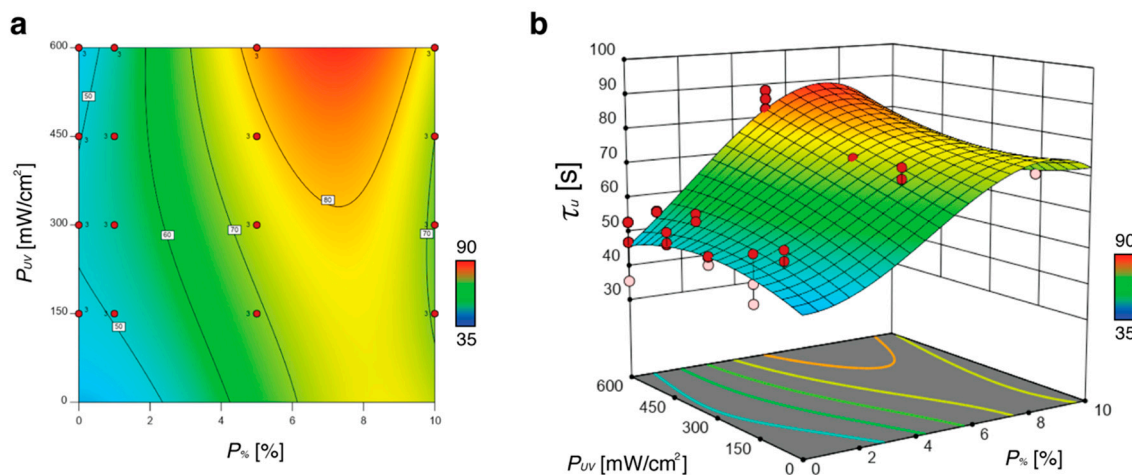


Figure 6. The value τ_u in the unbending process, drawn by the reduced cubic model. (a) Contour plot in 2D and (b) surface plot in 3D. The dark dots correspond to experimental data over the model response and light dots corresponds to experimental data below the model surface.

4. Conclusions

We fabricated hybrid silicones mixed with azobenzene powder, and enabled them to bend under UV light illumination due to the constraint by a paper. The photo-bending behavior of hybrid silicones was fitted with an exponential function, and then described by cubic models for A and τ_b with variables of the weight percentage of powder and the UV power, at least in the experimental range conducted in this work. Based on the constructed models, the amplitude A increases by both effects of the light intensity and the percentage of powder, and the time constant τ_b decreases by the light intensity but is susceptible to the percentage of powder in a not monotonous manner. The unbending behavior after turning off UV light was also observed, fitted with an exponential function, and then described by a simplified cubic model of the time constant τ_u . The model for unbending indicates that the value τ_u increases mainly due to the effect of the powder contents. This strategy from the experimental observations of actuation behavior to the description as a mathematical equation can be utilized for the optimization of the desired output, and for the programmed control by a computer. As for applications, the use and environment depend on the material properties. In order to use the presented solutions in real-life applications, a specific design has to be performed. Preferable use of the photo-bending property would be very gentle touch and grip of, for example, fragile objects. The actuation force is also an interesting parameter to be characterized, and this work will promote the development and implementation of photo-responsive materials for innovative actuators.

Supplementary Materials: The following are available online at <http://www.mdpi.com/2076-0825/8/4/68/s1>, Figure S1: Photo-actuation behaviors of a silicone monolayer of 1 wt% homogeneously mixed with azobenzene powder, Figure S2: Surface temperature change upon UV light irradiation, Figure S3: Unbending behaviors of the hybrid silicone of 10 wt% by thermal back and visible light irradiation, Table S1: Time dependence of the average of real deflection on three repetitions for photo-bending under light irradiation, Table S2: Time dependence of the average of real deflection on three repetitions for unbending after stopping light irradiation.

Author Contributions: Conceptualization, T.T., L.B., and P.L.; methodology, T.T. and L.B.; formal analysis, T.T. and L.B.; investigation, T.T.; resources, L.B. and P.L.; data curation, T.T.; writing—original draft preparation, T.T.; writing—review and editing, T.T., L.B., T.A., H.K., and P.L.; visualization, T.T. and L.B.; supervision, T.A., H.K., and P.L.

Funding: This study was financially supported by JSPS Grant-in-Aid for Scientific Research B (17H03107), Challenging Exploratory Research (16K12918), Research Fellowship for Young Scientists, Building of Consortia for the Development of Human Resources in Science and Technology and by the F.N.R.S. (Fonds National de la Recherche Scientifique) through an F.R.I.A. (Fonds pour la formation à la Recherche dans l'Industrie et dans l'Agriculture) grant, Research Project PDR T1002.14 and Research project PDR T0050.16.

Acknowledgments: T.T. and T.A. thank the Leading Graduate Program in Science and Engineering at Waseda University. T.T. is also thankful for the educational work at Building of Consortia for the Development of Human Resources in Science and Technology.

Conflicts of Interest: The authors declare no conflict of interest.

References

1. Capek, K.R.U. *R (Rossum's Universal Robots)*; Penguin Books: New York, NY, USA, 2004.
2. Rus, D.; Tolley, M.T. Design, fabrication and control of soft robots. *Nature* **2015**, *521*, 467–475. [[CrossRef](#)] [[PubMed](#)]
3. Laschi, C.; Mazzolai, B.; Cianchetti, M. Soft robotics: Technologies and systems pushing the boundaries of robot abilities. *Sci. Robot.* **2016**, *1*, eaah3690. [[CrossRef](#)]
4. Cianchetti, M.; Laschi, C.; Menciassi, A.; Dario, P. Biomedical applications of soft robotics. *Nat. Rev. Mater.* **2018**, *3*, 143–153. [[CrossRef](#)]
5. Yang, G.Z.; Fischer, P.; Nelson, B. New materials for next-generation robots. *Sci. Robot.* **2017**, *2*, eaap9294. [[CrossRef](#)]
6. Banerjee, H.; Suhail, M.; Ren, H. Hydrogel actuators and sensors for biomedical soft robots: Brief overview with impending challenges. *Biomimetics* **2018**, *3*, 15. [[CrossRef](#)] [[PubMed](#)]
7. Montero De Espinosa, L.; Meesorn, W.; Moatsou, D.; Weder, C. Bioinspired polymer systems with stimuli-responsive mechanical properties. *Chem. Rev.* **2017**, *117*, 12851–12892. [[CrossRef](#)] [[PubMed](#)]
8. Lv, J.A.; Liu, Y.; Wei, J.; Chen, E.; Qin, L.; Yu, Y. Photocontrol of fluid slugs in liquid crystal polymer microactuators. *Nature* **2016**, *537*, 179–184. [[CrossRef](#)] [[PubMed](#)]
9. Iwaso, K.; Takashima, Y.; Harada, A. Fast response dry-type artificial molecular muscles with [c2] daisy chains. *Nat. Chem.* **2016**, *8*, 625–632. [[CrossRef](#)]
10. Wani, O.M.; Zeng, H.; Priimagi, A. A light-driven artificial flytrap. *Nat. Commun.* **2017**, *8*, 15546. [[CrossRef](#)]
11. Lahikainen, M.; Zeng, H.; Priimagi, A. Reconfigurable photoactuator through synergistic use of photochemical and photothermal effects. *Nat. Commun.* **2018**, *9*, 4148. [[CrossRef](#)]
12. Kobatake, S.; Takami, S.; Muto, H.; Ishikawa, T.; Irie, M. Rapid and reversible shape changes of molecular crystals on photoirradiation. *Nature* **2007**, *446*, 778–781. [[CrossRef](#)] [[PubMed](#)]
13. Koshima, H.; Ojima, N.; Uchimoto, H. Mechanical motion of azobenzene crystals upon photoirradiation. *J. Am. Chem. Soc.* **2009**, *131*, 6890–6891. [[CrossRef](#)] [[PubMed](#)]
14. Taniguchi, T.; Fujisawa, J.; Shiro, M.; Koshima, H.; Asahi, T. Mechanical motion of chiral azobenzene crystals with twisting upon photoirradiation. *Chem. Eur. J.* **2016**, *22*, 7950–7958. [[CrossRef](#)] [[PubMed](#)]
15. Naumov, P.; Chizhik, S.; Panda, M.K.; Nath, N.K.; Boldyreva, E. Mechanically responsive molecular crystals. *Chem. Rev.* **2015**, *115*, 12440–12490. [[CrossRef](#)] [[PubMed](#)]
16. Taniguchi, T.; Asahi, T.; Koshima, H. Photomechanical azobenzene crystals. *Crystals* **2019**, *9*, 437. [[CrossRef](#)]
17. Lan, T.; Chen, W. Hybrid nanoscale organic molecular crystals assembly as a photon-controlled actuator. *Angew. Chem. Int. Ed.* **2013**, *52*, 6496–6500. [[CrossRef](#)] [[PubMed](#)]
18. Chandra Sahoo, S.; Nath, N.K.; Zhang, L.; Semreen, M.H.; Al-Tel, T.H.; Naumov, P. Actuation based on thermo/photosalient effect: A biogenic smart hybrid driven by light and heat. *RSC Adv.* **2014**, *4*, 7640–7647. [[CrossRef](#)]
19. Yu, Q.; Yang, X.; Chen, Y.; Yu, K.; Gao, J.; Liu, Z.; Cheng, P.; Zhang, Z.; Aguila, B.; Ma, S. Fabrication of light-triggered soft artificial muscles via a mixed-matrix membrane strategy. *Angew. Chem. Int. Ed.* **2018**, *57*, 10192–10196. [[CrossRef](#)] [[PubMed](#)]
20. Shi, Y.X.; Zhang, W.H.; Abrahams, B.F.; Braunstein, P.; Lang, J.P. Fabrication of photoactuators: Macroscopic photomechanical responses of metal–organic frameworks to irradiation by UV light. *Angew. Chem. Int. Ed.* **2019**, *58*, 9453–9458. [[CrossRef](#)]
21. Koshima, H.; Matsudomi, M.; Uemura, Y.; Kimura, F.; Kimura, T. Light-driven bending of polymer films in which salicylidenephenylethylamine crystals are aligned magnetically. *Chem. Lett.* **2013**, *42*, 1517–1519. [[CrossRef](#)]
22. Zhang, X.; Yu, Z.; Wang, C.; Zarrouk, D.; Seo, J.W.T.; Cheng, J.C.; Buchan, A.D.; Takei, K.; Zhao, Y.; Ager, J.W.; et al. Photoactuators and motors based on carbon nanotubes with selective chirality distributions. *Nat. Commun.* **2014**, *5*, 2983. [[CrossRef](#)] [[PubMed](#)]

23. Nakata, K.; Sakai, M.; Ochiai, T.; Murakami, T.; Fujishima, A. Bending motion of a polyacrylamide/graphite fiber driven by a wide range of light from UV to NIR. *Mater. Lett.* **2012**, *74*, 68–70. [[CrossRef](#)]
24. Deng, J.; Li, J.; Chen, P.; Fang, X.; Sun, X.; Jiang, Y.; Weng, W.; Wang, B.; Peng, H. Tunable photothermal actuators based on a pre-programmed aligned nanostructure. *J. Am. Chem. Soc.* **2016**, *138*, 225–230. [[CrossRef](#)] [[PubMed](#)]
25. Lee, E.; Kim, D.; Kim, H.; Yoon, J. Photothermally driven fast responding photo-actuators fabricated with comb-type hydrogels and magnetite nanoparticles. *Sci. Rep.* **2015**, *5*, 15124. [[CrossRef](#)] [[PubMed](#)]
26. Ahir, S.V.; Terentjev, E.M. Photomechanical actuation in polymer-nanotube composites. *Nat. Mater.* **2005**, *4*, 491–495. [[CrossRef](#)] [[PubMed](#)]
27. Hu, Y.; Li, Z.; Lan, T.; Chen, W. Photoactuators for direct optical-to-mechanical energy conversion: From nanocomponent assembly to macroscopic deformation. *Adv. Mater.* **2016**, *28*, 10548–10556. [[CrossRef](#)] [[PubMed](#)]
28. Niu, D.; Jiang, W.; Liu, H.; Zhao, T.; Lei, B.; Li, Y.; Yin, L.; Shi, Y.; Chen, B.; Lu, B. Reversible bending behaviors of photomechanical soft actuators based on graphene nanocomposites. *Sci. Rep.* **2016**, *6*, 27366. [[CrossRef](#)] [[PubMed](#)]
29. Van Oosten, C.L.; Harris, K.D.; Bastiaansen, C.W.M.; Broer, D.J. Glassy photomechanical liquid-crystal network actuators for microscale devices. *Eur. Phys. J. E* **2007**, *23*, 329–336. [[CrossRef](#)] [[PubMed](#)]
30. Cheng, L.; Torres, Y.; Min Lee, K.; McClung, A.J.; Baur, J.; White, T.J.; Oates, W.S. Photomechanical bending mechanics of polydomain azobenzene liquid crystal polymer network films. *J. Appl. Phys.* **2012**, *112*, 013513. [[CrossRef](#)]
31. Nath, N.K.; Pejov, L.; Nichols, S.M.; Hu, C.; Saleh, N.I.; Kahr, B.; Naumov, P. Model for photoinduced bending of slender molecular crystals. *J. Am. Chem. Soc.* **2014**, *136*, 2757–2766. [[CrossRef](#)]
32. Zhou, B.; Bernhardt, E.; Bhuyan, A.; Ghorbanishiadeh, Z.; Rasmussen, N.; Lanska, J.; Kuzyk, M.G. Theoretical and experimental studies of photomechanical materials. *J. Opt. Soc. Am. B* **2019**, *36*, 1492–1517. [[CrossRef](#)]
33. Koshima, H.; Ojima, N. Photomechanical bending of 4-aminoazobenzene crystals. *Dyes Pigment.* **2012**, *92*, 798–801. [[CrossRef](#)]



© 2019 by the authors. Licensee MDPI, Basel, Switzerland. This article is an open access article distributed under the terms and conditions of the Creative Commons Attribution (CC BY) license (<http://creativecommons.org/licenses/by/4.0/>).